Author Query Form

Journal : Cerebral Cortex

Article doi : 10.1093/cercor/bhp001

Article title : Functional Selectivity of Interhemispheric Connections in Cat Visual Cortex

First Author : N.L. Rochefort

Corr. Author : N.L. Rochefort

AUTHOR QUERIES - TO BE ANSWERED BY THE CORRESPONDING AUTHOR

The following queries have arisen during the typesetting of your manuscript. Please answer these queries by marking the required corrections at the appropriate point in the text.

Q1	Please check that reference Kisvárday and Eysel (1994) is not given in the reference list.	
Q2	Please check that reference Payne et al. (1991) is not given in the reference list.	
Q3	Please provide publisher name in reference Batschelet (1981).	

CERCOR	bhp001	SU
Journal Name	Art. No.	CE Code

Cerebral Cortex
doi:10.1093/cercor/bhp001

Functional Selectivity of Interhemispheric Connections in Cat Visual Cortex

N.L. Rochefort[1,2,3], P. Buzás[4], N. Quenech'du[3], A. Koza[5], U.T. Eysel[1], C. Milleret[3] and Z.F. Kisvárday[6]

[1]Department of Neurophysiology, MA 4/149, Ruhr-Universität, D-44780 Bochum, Germany, [2]International Graduate School of Neuroscience (IGSN), Ruhr-Universität, Bochum, Germany, [3]Laboratoire de Physiologie de la Perception et de l'Action, Collège-de-France, UMR CNRS 7152, 11 Place Marcelin Berthelot, 75005 Paris, France, [4]Institute of Physiology, University of Pécs, Pécs, Hungary, [5]Department of General Zoology and Neurobiology, University of Pécs, Pécs, Hungary and [6]Laboratory for Cortical Systems Neuroscience, Department of Anatomy, Histology and Embryology, University of Debrecen, Nagyerdei krt. 98, 4012 Debrecen, Hungary

The functional specificity of callosal connections was investigated in visual areas 17 and 18 of adult cats, by combining in vivo optical imaging of intrinsic signals with labeling of callosal axons. Local injections of neuronal tracers were performed in one hemisphere and eight single callosal axons were reconstructed in the opposite hemisphere. The distributions of injection sites and callosal axon terminals were analyzed with respect to functional maps in both hemispheres. Typically, each callosal axon displayed two or three clusters of synaptic boutons in layer II/III and the upper part of layer IV. These clusters were preferentially distributed in regions representing the same orientation and the same visuotopic location as that at the corresponding injection sites in the opposite hemisphere. The spatial distribution of these clusters was elongated and its main axis correlated well with the preferred orientation at the injection site. These results demonstrate a specific organization of interhemispheric axons that link cortical regions representing the same orientation and the same location of visual stimuli. Visual callosal connections are thus likely involved in the processing of coherent information in terms of shape and position along the midline of the visual field, which may facilitate the fusion of both hemifields into the percept of a single visual scene.

Keywords: area 17, area 18, callosal connections, corpus callosum, long-range connections, primary visual cortex

Introduction

In mammals with frontal eyes, each visual hemifield is represented in the visual cortex of the contralateral hemisphere. However, the central vertical meridian and its vicinity display a cortical representation in both hemispheres. These representations of the central part of the visual field are linked by long-range commissural connections through the splenial part of the corpus callosum (Choudhury et al. 1965; Berlucchi et al. 1967; Hubel and Wiesel 1967; Berlucchi and Rizzolatti 1968; Milleret and Buser 1993; Milleret et al. 1994; Payne 1994; Milleret et al. 2005). Regarding the intracortical termination of callosal connections, anatomical studies performed in monkeys, cats, and rats revealed a clustered organization (Houzel and Milleret 1999). In order to obtain a better understanding of the functional topography of the visual callosal pathway, an important step is to determine how these clusters of callosal connections relate to the different functional domains of the visual cortex. Do callosal axons link similar or dissimilar functional domains between the hemispheres? Do they differ from the long-range intrahemispheric excitatory network in which intracortical patchy connections have been associated with similar orientation domains in the visual cortex (Gilbert and Wiesel 1989; Malach et al. 1994; Buzás et al. 2006)?

A discontinuous "columnar" pattern of callosal connections has been reported many years ago in rats and monkeys (Heimer et al. 1967; Künzle 1976; Jones et al. 1979). The patchy distribution of callosal connections was later confirmed in the cat visual cortex at the level of callosal neurons population using bulk injections (Berman and Payne 1983; Innocenti 1986a; Voigt et al. 1988; Boyd and Matsubara 1994) as well as at the level of individual callosal axons using the anterograde tracer biocytin (Houzel et al. 1994; Aggoun-Zouaoui et al. 1996). In cats, this clustered organization is similar in size and shape to that of the patchy intracortical network (Kisvarday 1992; Kisvárday and Eysel 1992). Both callosal neurons and callosal terminals were shown to be densely packed within cytochrome oxidase-rich domains in the visual cortex of cats (Boyd and Matsubara 1994) and macaques (Olavarria and Abel 1996). Periodicities in the distribution of callosal neurons also appeared to correlate with the pattern of ocular dominance columns in cat visual cortex (Olavarria 2001; but see Schmidt et al. 1997).

Regarding the orientation selectivity of callosal connections, such selectivity has been suggested in studies of interhemispheric synchronizations in cat visual cortex (Engel et al. 1991). The activity of neurons recorded simultaneously in each hemisphere was synchronized when neurons had the same orientation preference. This synchronization was abolished by section of the corpus callosum (Engel et al. 1991; Nowak et al. 1995). More recent studies in ferret and humans also demonstrated that interhemispheric coherence increased when gratings with similar orientations were presented simultaneously in both hemifields (Kiper et al. 1999; Carmeli et al. 2005, 2007; Knyazeva et al. 2006; Makarov et al. 2008). These data support the hypothesis that temporal synchrony of neuronal discharges serves to bind features within and between the visual hemifields. However, the anatomical basis of these synchronizations could not be determined precisely. In order to investigate this issue, two studies combined retrograde labeling of callosal neurons with functional data (using 2-deoxyglucose autoradiography and optical imaging of intrinsic signals) but led to conflicting results. In one study, callosal connections were found to link similar orientation domains in the visual cortex of strabismic cats (Schmidt et al. 1997). In another study, callosal neurons labeled in the visual cortex of normal adult tree shrews did not correlate with the layout of orientation domains (Bosking et al. 2000). Instead,

these connections appeared to link visuotopically corresponding sites, suggesting that visuotopy is the primary factor constraining their distribution.

The functional specificity of callosal connections with respect to the map of visual space was investigated in cats and tree shrews using retrograde labeling of callosal neurons (Olavarria 1996; Bosking et al. 2000; Alekseenko et al. 2005). These studies revealed a nonhomotopic pattern of callosal connections that is compatible with a visuotopic organization of these connections. In cat visual cortex, callosal neurons located in A17 and A18 project their axon into the transition zone between A17 and 18 (transition zone [TZ]) in the other hemisphere, whereas callosal neurons located in the TZ project mainly into contralateral A17 and A18 (Olavarria 1996; Alekseenko et al. 2005). How this retinotopic organization of callosal connections is related to other functional features of the visual cortex such as ocular dominance and orientation preference domains remains to be determined. It has been shown that the spatial distribution of horizontal connections displays an axial specificity with regard to the retinotopic map in V1 of the tree shrew (Chisum et al. 2003; Fitzpatrick 1996; Bosking et al. 1997) and the New World Monkey (Sincich and Blasdel 2001). Similar functional organization was described for feedback projections from V2 to V1 in the owl monkey (Shmuel et al. 2005). These labeled connections extend along a retinotopic axis corresponding to the preferred orientation at the injection site. So far, no study has been published concerning the axial specificity of callosal axons.

In this study, the distribution of the synaptic boutons of individual callosal axons was investigated and compared with orientation maps of the visual areas 17 and 18 in normal adult cats. Optical imaging of intrinsic signals was combined with small extracellular iontophoretic injections of neuronal tracers (mainly anterograde) in one hemisphere and reconstructions of labeled callosal axons in the other hemisphere. We found that all callosal axons preferentially connected domains representing the same orientation and the same visuotopic location as that at the corresponding injection sites in the opposite hemisphere. Moreover, the axis of elongation of their termination fields correlated well with the preferred orientation of the site of origin in the opposite hemisphere. Part of this work has been published previously in abstract form (Rochefort et al. 2005).

Materials and Methods

Four normal adult cats (6, 7, 14, 22 months old) were used in this study. All surgical procedures conformed to institutional and governmental requirements (German Animal Welfare Act) and the guidelines of the European Convention for the Protection of Vertebrate Animals Used for Experimental and Other Scientific Purposes (Strasbourg, 18.III, 1986).

Surgical Procedures for Tracer Injections and Electrophysiological Characterization of the Injection Sites

Tracer injections were made 13–19 days prior to optical imaging recordings in order to allow sufficient time for interhemispheric transport of the tracers. For surgery, anesthesia was induced with a mixture of ketamine (10 mg/kg; Ketavet; Pharmacia and Upjohn, Erlangen, Germany) and xylazine (1 mg/kg, i.m.; Rompun; Bayer Belgium, Sint-Truiden, Belgium). The initial anesthesia was prolonged with halothane (0.4–0.6% of halothane; Halothane; Halocarbon, NJ) using tracheal intubation and artificial ventilation (1:2 mixture O_2 and N_2O). Vital parameters such as expiratory CO_2 (3.4–4%) and body temperature (38.5 °C) were monitored continuously. Before head surgery, the animal's skin was scrubbed with an antiseptic tincture and the head was installed in a stereotaxic apparatus. A craniotomy (2 × 3 mm) was made in the left hemisphere above the transition zone between A17 and A18, centered on stereotaxic (Horsley-Clarke) coordinates A0.5/L3. Extracellular iontophoretic injections were made at two locations spaced 1 mm apart along the antero-posterior axis of the small craniotomy. The tracer-filled glass micropipettes (GB100F-10; Science Products, Frankfurt/Main, Germany; tip diameter 10 μm) were advanced through a small slit on the dura mater 300–400 μm below the cortical surface. At one site, 5% of biotinylated dextran-amine (BDA, 10,000 MW; Molecular Probes, Leiden, Netherlands) and at the other site 5% of dextran tetramethylrhodamine (Fluoro-Ruby [FR], 10,000 MW; Molecular Probes) in 0.1 M phosphate-buffered saline (PBS; pH = 7.6) were injected by passing positive 2 μA (500 ms ON/500 ms OFF duty cycle, square-wave) for 20 min.

Before starting the iontophoretic injection, multiunit recordings were made via the same glass pipettes. The visuotopic location of the receptive fields and the preferred orientations were determined using hand-held visual stimuli. At the end of the experiment, the piece of bone flap that had been taken out from the craniotomy and kept in Ringer solution was put back on the dural surface and sealed with bone wax. The skin was folded over and sewed with surgical thread. Antiseptic ointment (Betaisodona; Mundipharma, Germany) was applied locally on the surgical wound and antibiotic (0.5 mL/5 kg; Tardomyocel; Bayer Vital, Leverkusen, Germany) injected i.m. Intubation was stopped after signs of spontaneous breathing and the animal was helped recovering in the animal house until optical imaging recordings. On the first day of recovery, a nonsteroidal anti-inflammatory agent was given i.m. (1 mL/10 kg, Tolfedine 4%; Vétoquinol, Goch, Germany).

Surgical Procedures for Optical Imaging and Electrophysiological Recordings from the Terminal Zone of Callosal Connections

The animals were prepared for surgery using standard procedures described previously (Buzás et al. 1998; Yousef et al. 1999). Anesthesia was induced with a mixture of ketamine (10 mg/kg; Ketavet; Pharmacia and Upjohn) and xylazine (1 mg/kg, i.m.; Rompun; Bayer Belgium). Neutral contact lenses and eye drops (1.5% saline) were used to protect the corneas from drying. The femoral artery was cannulated in order to monitor blood pressure (95–140 mm Hg) and to infuse a mixture of muscle relaxant (alcuronium chloride; 0.15 mg/kg/h; Alloferin, ICN Pharmaceuticals, Frankfurt/Main, Germany) and glucose (24 mg/kg/h; Glucosteril; Fresenius Kabi, Bad Homburg, Germany) in Ringer solution (Ringerlösung; Fresenius Kabi). A tracheal cannula was implanted for prolonged anesthesia (0.4–0.6% of halothane; Halothane; Halocarbon) and artificial ventilation (1:2 mixture O_2 and N_2O). Expiratory CO_2 (3.4–4%), body temperature (38.5 °C) and EEG were monitored continuously.

A craniotomy was performed on both hemispheres between stereotaxic coordinates (Horsley–Clarke) P7–A12 and L0.5–L6.5 in order to expose the cortical region corresponding to the representation of the central and lower parts of the visual field in both A17 and A18 (Tusa et al. 1978, 1979). A round metal chamber (31 mm inner diameter) was mounted onto the skull using dental cement (Paladur; Heraeus Kulzer, Wehrheim, Germany) and bone screws placed in the frontal bone. Then, the dura mater was removed, the chamber filled with silicone oil (50 cSt viscosity; Aldrich, Milwaukee, WI) and sealed with a round coverglass.

Shortly before starting optical imaging, the nictitating membranes were retracted with 5% phenylephrinhydrochloride (Neosynephrin-POS; Ursapharm, Saarbrücken, Germany) and the pupils were dilated with 1% atropine sulfate (Atropin-POS; Ursapharm). Correction lenses for a viewing distance of 28.5 cm were applied on the basis of tapetal reflection.

Optical Imaging of Intrinsic Signals

Visual Stimulation

Visual stimuli were generated with the stimulus generator VSG Series Three system (Cambridge Research Systems, Rochester, UK) and presented on a video screen at 100 Hz in noninterlaced mode at a distance of 28.5 cm in front of the cat's eyes.

By using an ophthalmoscope, the locations of the optic disks and of the area centralis of each eye were back-projected onto the video screen placed at 28.5 cm in front of the animal's eyes. Thereafter, the video screen was centered on the estimated vertical midline and its height adjusted to place the location of area centralis in the upper one third. In this way, both the central and the lower part of the visual field were stimulated, that is, the region represented in the most part of the imaged cortical region (rostral part of A17 and adjoining A18). The vertical midline was defined as the vertical line crossing the area centralis, and the latter corresponded to the retinal area devoid of blood vessels. The position of the vertical meridian was confirmed by controlling the geometrical relation between the area centralis, the vertical midline and the optic disk (Bishop et al. 1962).

For orientation maps, the stimuli consisted of full-field, high-contrast, square-wave luminance gratings that moved back and forth along the orthogonal axis of the orientation in either direction for half of the data acquisition period. A single stimulus trial consisted of gratings of four or eight equally spaced orientations (0, 45, 90, 135 deg and 0, 22.5, 45, 67.5, 90, 112.5, 135 deg, respectively) at spatial and temporal frequencies (generally, 0.15 cpd, 1.5 Hz, i.e., 10 deg/s) that resulted in the strong activation of the part of the visual cortex where most transcallosal connections are located.

The transition zone between A17 and A18 (TZ) was determined on the basis of activity maps obtained with visual stimuli presented at different spatial and temporal frequencies. For A17 activation, luminance gratings of four or eight equally spaced orientations were displayed at 0.6 cpd spatial and 1.5 Hz temporal frequencies (i.e., 2.5 deg/s) whereas for A18 the respective frequencies were 0.15 cpd and 4.5 Hz (i.e., 30 deg/s) (Bonhoeffer et al. 1995; Rochefort et al. 2007).

For mapping iso-elevation lines (vertical eccentricity), images were acquired during the presentation of a narrow horizontal bar (width 1°) containing a moving vertical grating (0.15 cpd, 1.5 Hz; i.e., 10 deg/s) at 13 different positions (degrees of elevation: +2, 0, −2, −4, −6, −8, −10, −12, −14, −16, −18, −20, −22). In all positions, the grating was moving along a horizontal axis, in one direction for half of the data acquisition period and then in the opposite direction. Negative and positive values corresponded to the lower and the upper visual hemifield respectively; 0° corresponded to the horizontal meridian. The presence of residual eye movements in paralyzed cats (Chow and Lindsley 1968; Bishop et al. 1971) can modify the location of the vertical meridian. These movements were controlled in each experiment by regularly plotting the optic disks, the area centralis and easily identifiable intersections of blood vessels. In the present study, apparent shifts in eye positions appeared only during long recording sessions (approximately 5–6 h). The magnitude of these movements was approximately 1–2°. In these cases, the results of the retinotopic mapping were corrected.

All stimuli were displayed in a pseudorandom sequence and presented 50–225 times for orientation and spatial frequency maps and 450–1500 times for retinotopic maps, depending on the experiment. Each eye was thus stimulated between 13 and 58 min per imaging session for orientation and spatial frequency maps and between 1 h, 56 min and 6 h. 28 min for retinotopic maps, depending on the level of activation of the visual cortex during recordings.

Data Acquisition

Optical imaging of intrinsic signals was carried out using the Imager 2001 imaging system (Optical Imaging, Inc.) and the data acquisition software VDAQ (NT version 1.0.1.0293, Optical Imaging, Mountainside, NJ) (for a detailed description, see Buzás et al. 1998; Yousef et al. 1999). Briefly, the cortex was illuminated with a circular fiber optic slit lamp (Schott, Mainz, Germany) surrounding the camera optics (two SMC Pentax lenses, 1:1.2, $f = 50$ mm, arranged in a tandem manner; Ratzlaff and Grinvald 1991). For simultaneous imaging of the two hemispheres, a converter (1:2, AF Telekonverter C/D7, Soligor, Leinfelden-Echterdingen, Germany) was added in front of the tandem lenses.

The vascular pattern of the cortical surface was imaged using 545 ± 10 nm (green) light before and after each recording session. During data acquisition, the cortex was illuminated with 609 ± 5 nm (orange) light and the camera focused 700–750 μm (for optics of 1:1 magnification) or 900–1000 μm (for 1:2 magnification) below the cortical surface. During interstimulus intervals (10 s), the animal viewed a stationary image of the next stimulus to be moved. Data acquisition commenced 1 s after the stimulus grating began to drift. Camera frames were recorded for 4.5 s at 25-Hz rate, using a Teli CS8310C camera (Tokyo Electronic Industries, Tokyo, Japan), when the grating moved along the orthogonal axis of the orientation alternatively in one direction and the other for exactly the same duration. The camera frames were summed temporally into 10 data frames (0.9 s per data frame). The spatial resolution of the final images was 21.28 × 21.28 μm per pixel.

Calculation of the Functional Maps

Single-condition maps (SCMs) were calculated by summing the images associated with a particular attribute of the visual stimulus (orientation, spatial frequency, azimuth position, or stimulated eye) using the MIX software (Optical Imaging, Inc.). All SCMs were divided by the sum of images recorded for all stimulus conditions (cocktail blank) (see Bonhoeffer and Grinvald 1993, 1996). The gray value distribution of the image pixels of each SCM was clipped by discarding extreme values outside the range defined as ±2–3 times the mean absolute deviation around the mean. The SCMs were then scaled to gray values with a range between 0 and 255. In the resulting images, low gray values (dark patches) corresponded to functional domains that were activated by a given stimulus (Bonhoeffer and Grinvald 1996). Further analysis of the images was made using custom-made software written in IDL (Research Systems, Boulder, CO). The SCMs were filtered using a Laplace filter (high-pass, 50 pixels kernel) to remove low-frequency noise resulting from uneven illumination, followed by a boxcar filter (low-pass, 5–11 pixels kernel). Angle maps were calculated using a pixel-by-pixel vectorial summation of SCMs. The angle of the resulting vector, indicating the preferred orientation, was displayed as the hue of each pixel.

Reference Penetrations

After optical imaging, 5–10 reference penetrations were made in each hemisphere. They were used for the alignment of the optical images with the sections containing the labeling. To this end, empty glass micropipettes (10–15 μm tip diameter) were lowered 1000 μm deep into the cortex parallel to the optical axis of the imaging camera and then withdrawn (Kisvárday and Eysel 1994). The lateral separation of the penetrations was 500–1500 μm. The exact locations of the entry points of the pipettes were marked on an enlarged printout of the image of the cortical surface. In this way, the microlesions caused by the pipettes in the cortical tissue could be localized in histological sections.

Histological Procedures

At the end of the experiment, animals received an overdose of anesthetics and were perfused transcardially with Tyrode's solution followed by a mixture of 4% paraformaldehyde (Merck, Darmstadt, Germany) and 0.1% glutaraldehyde (Merck) in 0.1 M phosphate buffer solution (PB, pH = 7.6). Blocks of cortex containing the optically imaged regions were dissected and cut in 60-μm-thick horizontal sections using a vibratome. Part of the corpus callosum corresponding to the antero-posterior extent of the cortical blocks was also dissected and placed in sucrose solutions (10%, 20%, and 30%) until it sank. Thereafter, 72-μm-thick frozen sections were cut in a parasagittal plane using a cryotome. For distinguishing the labeling by the two tracers, all sections from left and right cortex were double-stained to BDA (in light-brown) and FR (in bluish black) (Fig. 1). For sections of the corpus callosum, BDA and FR labeling was revealed, respectively, in alternate sections.

BDA labeling was revealed using the avidin-biotin-complexed horseradish peroxidase (ABC; Vector Laboratories, Burlingame, CA) method. The sections were washed for 2 × 20 min in 0.1 M PB and incubated in ABC 1:200 in 0.1 M Tris-buffered saline solution (TBS; pH = 7.6) at 4 °C, overnight. Enzymatic reaction was revealed with 0.05% 3,3′-diaminobenzidine-4-HCl (DAB; Sigma-Aldrich, Deisenhofen, Germany) in TRIS (pH = 7.6) for 20 min and completed in the presence of 0.0025% H_2O_2 for 1–3 min.

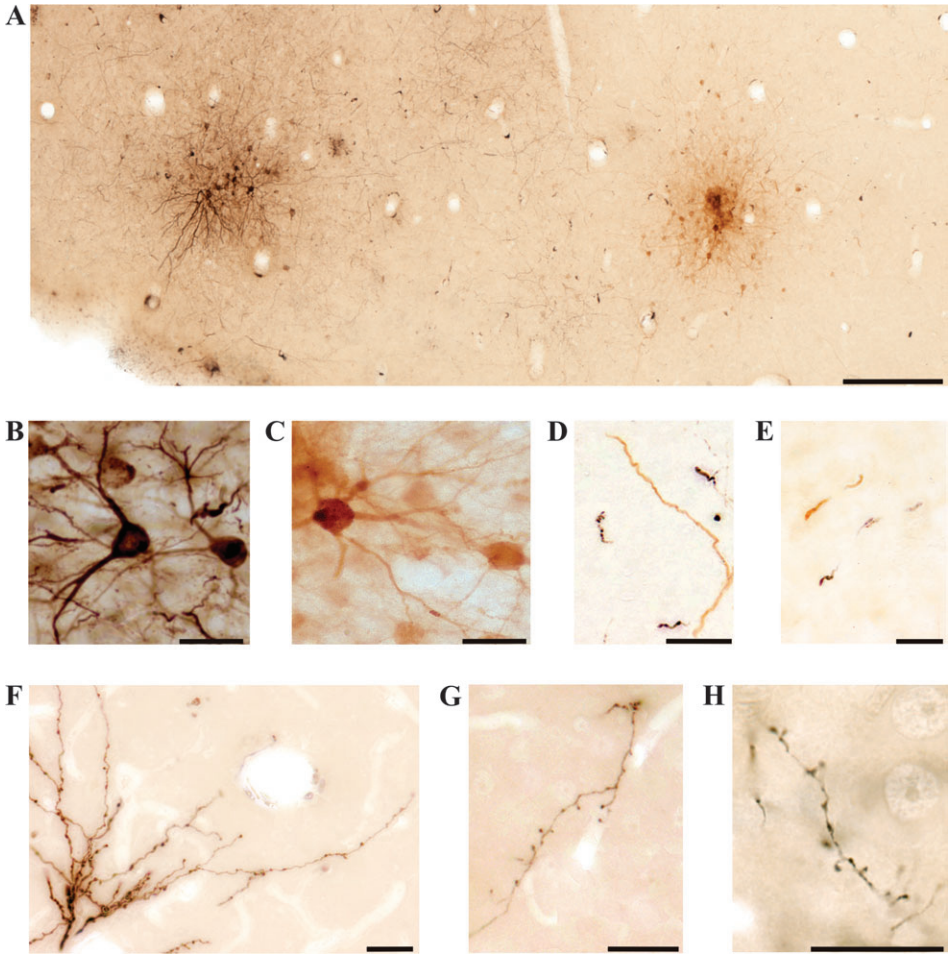

Figure 1. Light microscopic images of neurons labeled with FR and BDA. Each tracer was revealed in one color: black for FR and light-colored brown for BDA. (*A–C*) Two injection sites in cat Ca09 (left hemisphere), located 240 μm (*A*, *C*), and 360 μm (*B*) below the cortical surface. The two colors can be clearly distinguished in A and at higher magnifications in (*B*) and (*C*) (FR and BDA, respectively). (*D*, *E*) Labeled callosal axons in deep cortical sections not treated with osmium, in the right hemisphere of cat Ca09, located 1200 μm (*D*) and 2280 μm (*E*) below the cortical surface. The deep cortical sections were not treated with osmium in order to determine the origin of labeled callosal axons according to their color: the injection site of FR (black) or of BDA (light-colored brown). (*F–H*) Labeled callosal axons in superficial sections treated with osmium. (*F*) Cat Ca15, depth: 1020 μm; (*G*, *H*) Cat Ca09, depth: 600 and 960 μm, respectively. Scale bars, 250 μm (*A*); 25 μm (*B–H*).

Subsequent FR labeling was revealed using a rabbit anti-tetramethylrhodamine antiserum (1:5000; Molecular Probes, Leiden, Netherlands) diluted in 0.1 M PBS (pH = 7.6) containing 2% Normal Goat Serum at 4 °C, overnight. Sections were washed two times in PBS for 10 min and incubated with the secondary antiserum (1:200, peroxidase anti-rabbit; Vector Laboratories, Burlingame, CA) in PBS at 4 °C, overnight. Enzymatic reaction (0.05% DAB in TRIS) was supplemented with 0.005% $CoCl_2$ or 0.6% Nickel-sulfate intensification (Adams 1981; Hancock 1984) for 20 min and completed in the presence of 0.0025% H_2O_2 for 1–3 min. All reagents and solutions for revealing BDA and FR labeling contained 0.2% Triton X-100.

After light microscopic inspection of the wet sections, the top 20 sections from the cortical surface containing the entire gray matter and part of the underlying white matter were processed for resin embedding. In one animal (case Ca09), sections of only the right hemisphere were processed in this way. Accordingly, sections were rinsed in TRIS for 2 × 15 min and PB for 2 × 15 min, postfixed in 0.5% OsO_4 in 0.1 M PB for 10–20 min and dehydrated in an ascending series of ethanol followed by 2 × 15 min in propyleneoxide. Finally, sections were embedded in Durcupan ACM (Fluka, Neu-Ulm, Germany) and mounted on microscopic slides (Somogyi and Freund 1989). The remaining sections containing the white matter and sections of the corpus callosum were not treated with osmium. Instead, they were dry-mounted on chrome-gelatine–coated slides, rinsed 2 × 10 min in Xylene and coverslipped in DePeX (ERVA Finebiochemica GmbH KG, Heidelberg, Germany). These sections served to determine the origin of labeled callosal axons according to their color (Fig. 1*D*,*E*) deriving from the BDA (light-colored brown) or FR (bluish black) (Fig. 1*A–C*) injection sites.

Three-Dimensional Reconstructions

Eight labeled callosal axons of the right hemispheres (contralateral to the injection sites) were reconstructed in three-dimensions using a light microscope (Leica DMRB) at ×1000 magnification and the neuron reconstruction system, Neurolucida (MicroBrightField, Colchester, VT). The axons and their synaptic boutons (club-like and en-passant) were traced in the entire depth of the cortex and partly in the white matter using the most superficial 20 sections which were resin embedded and the adjoining 10–20 sections of the white matter which were dry-mounted, hence preserving the different coloring of BDA and FR labeling. Neighboring sections were aligned with the help of corresponding cut ends of labeled axonal processes and small blood vessels (<20 μm diameter) providing a 5- to 50-μm matching accuracy (Kisvárday et al. 1997).

In order to match the anatomical reconstructions with the optical images, the reference penetrations and the layout of surface blood vessels were also reconstructed. Finally, the borders of cortical layers were determined on the basis of relative density of neuronal cell bodies and fibers, soma size and the presence of layer-specific cell types, such as large pyramidal cells in lower layer III upper IV and giant pyramidal cells in layer Vb.

Alignment of the Reconstructed Axons and Injection Sites with the Optical Maps

All 3D-reconstructions were corrected for optical shrinkage in the *Z*-axis caused by the optical density of the embedding medium (epoxy resin) and the microscope immersion oil. The *Z*-values were multiplied by the correction factor, $f = n_{resin}/n_{oil} = 1.0204$, where n_{resin} and n_{oil} correspond to the index of refraction of the epoxy resin and the immersion oil, respectively (Buzás et al. 1998). Then, 3D-reconstructions were tilted and rotated into the plane of the optical images using reference penetrations, which ran parallel to the optical axis of the imaging camera. During the histological procedure, the sections underwent shrinkage, mainly due to dehydration. Therefore, the reconstructions were corrected for this type of shrinkage. It was then possible to match the anatomical reconstructions with the optical images with the help of the entry points of reference penetrations and the layout of the surface blood vessels (Buzás et al. 1998). This aligning method has an estimated error inferior to 50 μm (Yousef et al. 1999). Finally, the reconstructions had to be scaled to the size and resolution of the optical images. The pixel resolution of the optically recorded maps was 21.28 × 21.28 μm^2 and the 3D reconstructions were binned into the same pixel format. To this end, the reconstructions were overlaid with a grid of the same size as that of optical images and the number of axon terminals was counted in every pixel. The resulting bouton density maps permitted a direct comparison between the distribution of synaptic boutons and the functional maps on a pixel-by-pixel basis.

Data Analysis

Each reconstructed axon was analyzed with Neurolucida and Neuroexplorer software (MicroBrightField, Colchester, VT) in order to determine the main morphometric parameters such as the total length of each axon's arbor as well as the number and the coordinates of their synaptic boutons in layers II/III, IV, and V/VI. The cortical layers were identified on the basis of cells morphology.

In addition, the functional topography of individual callosal axons was determined using custom-made software written in IDL (Research Systems). The number of synaptic boutons in each orientation domain was calculated using a resolution (bin size) of 22.5°. For their analysis, the data were normalized in order to enable a direct comparison between individual cases. First, orientation preferences of the boutons were expressed relative to that of the injection sites resulting in values between –90° and +90°. Second, the number of boutons was expressed as a percentage of the total number of boutons for each axon. Their distributions in terms of orientation preference were divided according to iso- (±30°), oblique- (±30–60°) and cross- (±60–90°) orientation categories with respect to the orientation preferences of the injection sites.

Axial Specificity of Callosal Connections

The 17/18 TZ was determined on the basis of spatial frequency preference maps by dividing the sum of the four or eight SCMs obtained with the "A18 specific stimuli" by the sum of the four or eight SCMs obtained with the "A17 specific stimuli." In the resulting differential maps, the change in spatial frequency preference was defined according to the length of the gradient vectors after smoothing (Ohki et al. 2000). The 1-mm-wide region of pixels with long gradient vectors was considered to represent the 17/18 transition zone (Ohki et al. 2000).

The preferred axes of the spatial distribution of each callosal axon terminals were determined in a Cartesian coordinate system, based on the 2D coordinates (*x*, *y*) of the corresponding synaptic boutons, viewed in the plane tangential to the cortical surface (horizontal plane). The coordinates of the boutons were obtained from the 3D reconstruction of each callosal axon, using Neurolucida and Neuroexplorer softwares (MicroBrightField, Colchester, VT). For each axon, the first and the second principal components of the set of *x* and *y* coordinates were calculated. The first component corresponded to the principal axis of elongation of the distribution, whereas the second component was orthogonal to the first one. The first and the second principal components defined a Cartesian coordinate system to which the coordinates of each bouton were projected. The SD of the projections to the first principal axis was divided by the SD of the projections to the second principal axis (orthogonal axis). This value was used as a measure of elongation of the axon terminals distribution.

The preferred axis of the callosal axon terminals was then defined as the angle between the principal axis of the boutons distribution and the axis of the TZ in the region of the axon (see red and black dotted axes, respectively, in Fig. 7*E*). On the basis of the retinotopic organization of both the TZ (Payne 1990) and the neighboring cortical regions A17 and A18 (Tusa et al. 1978, 1979), this preferred axis was related to the portion of the visual field represented in the region of the axon. Because the visual vertical midline is represented along the TZ, a preferred axis of elongation parallel to the TZ corresponded to the representation of a vertical part of the visual field (see axon 4 in Fig. 7), whereas a preferred axis orthogonal to the TZ corresponded to the representation of a horizontal part of the visual field (see axon 3 in Fig. 7). We assumed, for simplicity, that the representation of horizontal lines (i.e., the iso-elevation lines) was orthogonal to the TZ and that the magnification factors were equal in all directions (Tusa et al. 1978, 1979; Payne 1990). To test the first assumption, we mapped the representation of iso-elevation lines in two animals (Ca09 and Ca15), an example of which is shown in Supplementary Figure 1. These maps supported our assumption that iso-elevation lines are mapped orthogonally to the TZ. Finally, the preferred axis of callosal axon terminals within the retinotopic representation of the visual space was compared with the orientation preference at the corresponding injection sites in the opposite hemisphere.

Results

The topographic relations between eight individual callosal neurons and functional maps of cat visual cortex (areas 17 and 18) were investigated at the level of both callosal cell bodies and terminal arbors within the left and the right hemisphere, respectively.

Morphological Characteristics of Individual Callosal Axons

Eight callosal axons were selected for three-dimensional reconstructions on the basis of strong synaptic bouton labeling (see e.g., Fig. 1*F–H*). The morphological characteristics of these axons terminal arbors are summarized in Table 1.

The entire intracortical ramification of each axon was reconstructed as well as the main axonal trunk, down to 317- to 722-μm-depth within the white matter (see Figs 2*A–C* and 3*B*). The total axonal length (including all branches) of these callosal axons varied from 11.2–31.2 mm. The total number of synaptic boutons ranged between 307 and 766. Most of these synaptic boutons were located in layer III (Table 1, Figs 2*A–C* and 3*B*) and approximately one third in layer IV. Only a few boutons were found in layer V/VI. When viewed in the plane tangential to the cortical surface (horizontal plane), the eight axons presented two or three distinct clusters of synaptic boutons (average diameter of 494 ± 146 μm, Figs 2*D–F* and 3*A*). These clusters were in most cases separated from each other by bouton free zones with a typical lateral spacing of 978 ± 327 μm except in axon 8 where the two clusters were adjacent.

When viewed in the frontal plane, the axons presented different branching patterns among which two main types could be distinguished (Figs 2*A–C* and 3*B*). These types were reminiscent of the architectures of callosal axons that have been previously described in cat visual cortex (Houzel et al. 1994). The eight axons displayed a parallel-type architecture (Figs 2 and 3), with long branches that ascend quasi-parallel to each other either in the white matter or in deep cortical layers, and supply different clusters of synaptic boutons. One axon (axon 8) displayed two close-by clusters linked to each other by a dense projection of axon collaterals.

Table 1
Experimental parameters and morphological characteristics of the reconstructed callosal axons

Cat	Age (months)	Tracer	Axon number	Total length (mm)	Callosal synaptic boutons (RH)				Anisotropy
					Total number	Layer II/III	Layer IV	Layer V/VI	
Ca06	14	BDA	1	12.98	508	482	7	19	10.4
			2	17.18	307	250	7	50	2.4
Ca07	6	FR	3	18.85	592	370	190	32	3.6
Ca09	22	BDA	4	13.95	616	549	46	21	2.1
			5	18.70	328	208	101	16	2.1
		FR	6	11.22	510	269	195	43	3.1
			7	21.72	761	621	112	25	4.2
Ca15	7	BDA	8	31.20	766	674	85	7	2.0

Note: The last column (anisotropy) shows a measure of elongation of the axon terminals distribution. The first and the second principal components of the synaptic bouton distributions defined a Cartesian coordinate system to which the coordinates of each bouton were projected. The standard deviation (SD) of the projections to the first principal axis was divided by the SD of the projections to the second principal axis (orthogonal axis). RH, right hemisphere.

Topographic Relations between Callosal Neurons and Orientation Maps

The orientation preference at the injection sites (labeled somata in left hemispheres) was compared with the orientation preference at the corresponding target zones of the labeled callosal axons (right hemispheres).

Orientation Selectivity at the Injection Sites (Left Hemispheres)

The orientation preference encoded at the injection sites was systematically determined by multiunit recordings via the tracer-filled glass pipette (Fig. 4*A*). In addition, in 4 out of 5 cases, orientation preference at the injection site was calculated from the distributions of the labeled neuronal somata (Fig. 4*B–E*) as well as from the location of the injection core in the orientation maps. The limited size of the injection sites in which injection cores varied from 230 to 393 μm in diameter (white circle in Fig. 4*D,E*) allowed such quantification. In the remaining case (Ca07), damage to the cortical surface (subdural blood clot) prevented us from obtaining orientation maps in the injected hemisphere. The orientation preference was thus established solely on the basis of electrophysiological recordings.

As a consequence of the limited size of the injections sites, the distributions of labeled neuronal somata (Fig. 4*H* and black bars in Fig. 4*I,J*) were, in all cases, centered on one given orientation (*V*-test [modified Rayleigh test]; $P < 0.01$, Batschelet 1981). Therefore, the circular mean (angle of the vector sum) was used as the preferred orientation of the injection sites. The resulting values were very close to the orientation represented in the region of the injection cores, as shown by the distribution of the pixels in the orientation maps of these regions (gray bars in Fig. 4*I,J*). It should be noted that the orientation preferences determined from the orientation maps corresponded well with the orientation preferences determined by electrophysiological recordings (maximum difference of ± 12°).

Orientation Selectivity at the Callosal Terminal Zones (Right Hemispheres)

The clusters of callosal terminal boutons were mainly located in orientation domains with the same orientation preference as that of the corresponding injection site. Figure 5 shows two examples of axons that connected similar orientation domains (0° for axon 1, 112.5° for axon 7), with two clusters of boutons for each axon. In order to demonstrate such specificity for the eight reconstructed axons, orientation preferences were expressed relative to that of the injection sites using 22.5° resolution (Fig. 5*B,C*). All eight bouton distributions were centered on 0° orientation difference between injection sites and terminal zones (*V*-test; modified Rayleigh test; $P < 0.01$).

Following the conventions used in earlier studies (Buzás et al. 2001; Kisvárday et al. 2002; Yousef et al. 1999), the orientation preference distribution of the synaptic boutons was determined according to iso- (±30°), oblique- (±30–60°) and cross- (±60–90°) orientation categories with respect to the orientation preference of the injection sites. The results showed that, on average, 72% (standard deviation = 17) of the boutons of the eight callosal axons were located in iso-orientation domains (Fig. 5*D*, Table 2). Some neurons appeared more iso-orientation selective (axons 1, 3, 7 with more than 83% of boutons in iso-orientation domains) than others (axons 2 and 5 with 50% and 51% of boutons in iso-orientation domains). This difference did not depend on the distance between the corresponding injection site and pinwheel centers in the orientation maps. It should be noted, however, that the two axons with the lowest percentage of iso-connections also had the lowest number of synaptic boutons, although the quality of their labeling did not differ from that of the other axons.

Retrograde Labeling of Callosal Neurons (Right Hemispheres)

Retrogradely labeled somata were also observed in the right hemispheres contralateral to the injection sites. The number of retrogradely labeled callosal neurons ranged between 3 and 11 within the four hemispheres that were analyzed (Table 2). These labeled somata were located in the same cortical region as the callosal axon terminals that were anterogradely labeled from the same injection site. Importantly, in four out of five cases (Ca06, Ca07, Ca09a, and CA09b), more than 50% of these labeled somata were found in iso-orientation regions (Fig. 6, Table 2). In the case of Ca15, the three labeled somata were distributed evenly in the three (iso-, oblique-, and cross-) orientation categories.

Topographic Relations between Callosal Neurons and Representation of the Visual Field in A17, A18, and TZ

Previous investigations with retrograde labeling of callosal neurons in cat visual cortex revealed a nonhomotopic pattern of callosal connections (Olavarria 1996): axons originating from the transition zone between A17 and 18 (TZ) project into contralateral regions outside the TZ (i.e., A17 and A18) whereas axons originating from regions outside the TZ project into the contralateral TZ. In the present study, the respective locations of the injection sites and the callosal axon terminals within A17, A18, and the TZ were also compared (Table 2). The TZ was localized in optically imaged activity maps based on the different spatial and temporal frequency preferences of A17 and A18 neurons (Fig. 7*C,D*) (Bonhoeffer et al. 1995; Rochefort et al. 2007).

In one animal (Ca06), the tracer's injection was performed in the TZ and resulted in labeled axons in the contralateral A17. In another animal (Ca15), the injection in A18 gave rise to labeled callosal axons in the TZ (Fig. 7*A*). These two cases were in agreement with the nonhomotopic pattern of callosal

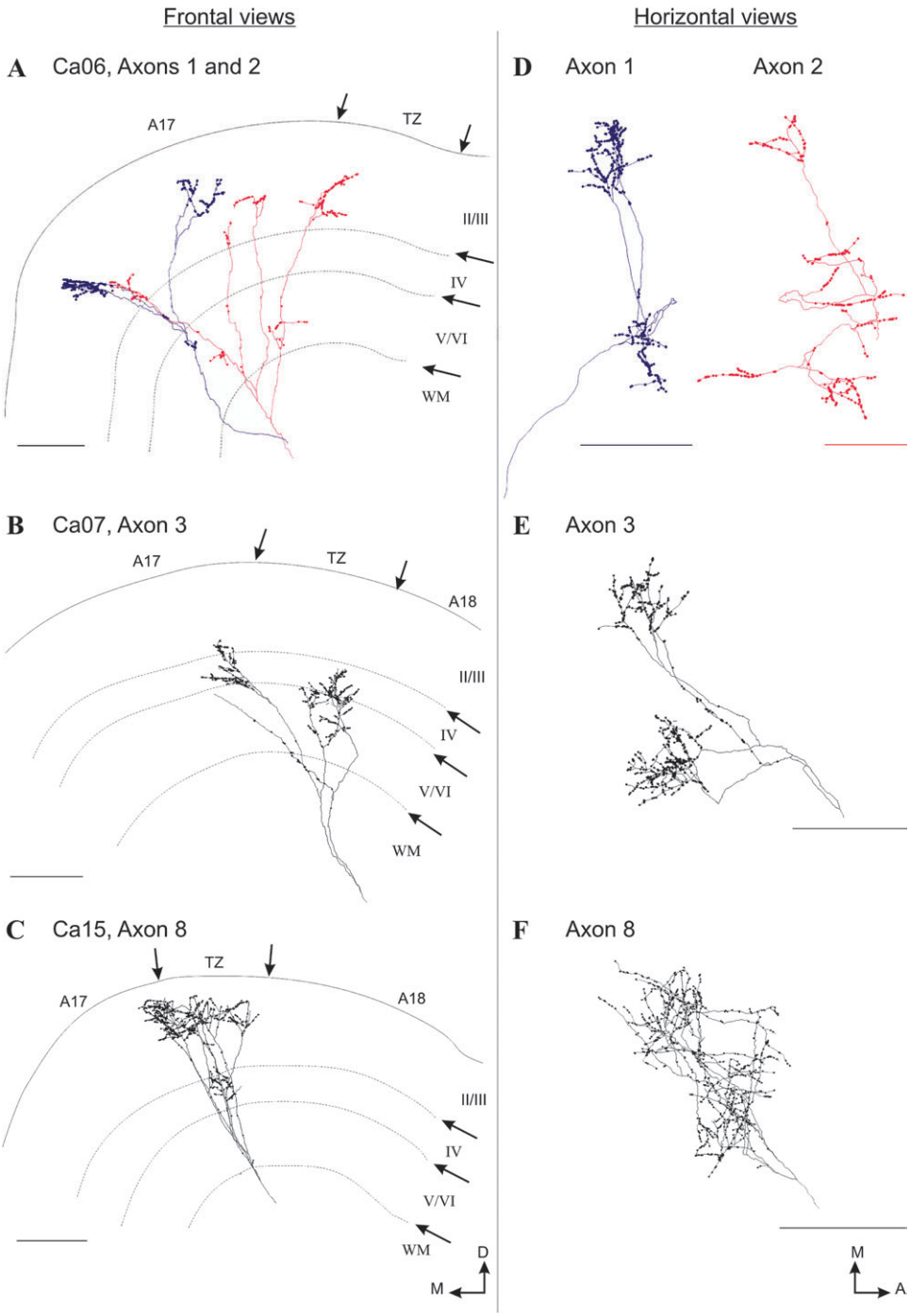

Figure 2. Three-dimensional reconstructions of callosal axon terminals (in right hemispheres). (*A–C*) Frontal views of axons 1 and 2 (cat Ca06), axon 3 (cat Ca07), and axon 8 (cat Ca15). The limits of cortical layers II/III, IV, V/VI, and of the white matter (WM) are indicated. The arrows at the top of each panel point the location of the 1-mm-wide TZ between A17 (on the right) and A18 (on the left). These limits (cortical layers and TZ) are those observed in one frontal plane at an antero-posterior level corresponding approximately to the center of the callosal axon's extent in the horizontal plane (Horsley–Clarke coordinates: P2 for axons 1 and 2; A1 for axon 3; A3 for axon 8). (*D–F*) Horizontal views (in a plane parallel to the cortical surface) of the same axons. A, anterior; D, dorsal; M, medial. Scale bars, 500 μm.

connections mentioned above (Olavarria 1996). In the last two animals, Ca07 and Ca09a, both injection sites and labeled axons were located in the TZ (Fig. 7*C*). Taking into account that the vertical meridian and a strip of the ipsilateral visual field are represented into the TZ (Fig. 4*A*; Diao et al. 1990; Payne 1990), these observations are compatible with the hypothesis of a visuotopic organization of callosal connections. Nonetheless, more examples of labeled callosal axons combined with detailed retinotopic mapping would be needed to determine the precise relationship of callosal connections with the representation of the visual field in TZ and neighboring A17 and A18.

Our data are consistent with the prediction that changes in cortical magnification between TZ, A17, and A18 should be reflected in the morphology of individual callosal axons targeting these regions (Olavarria 1996). Due to the compression of ipsilateral visual field representation within the TZ

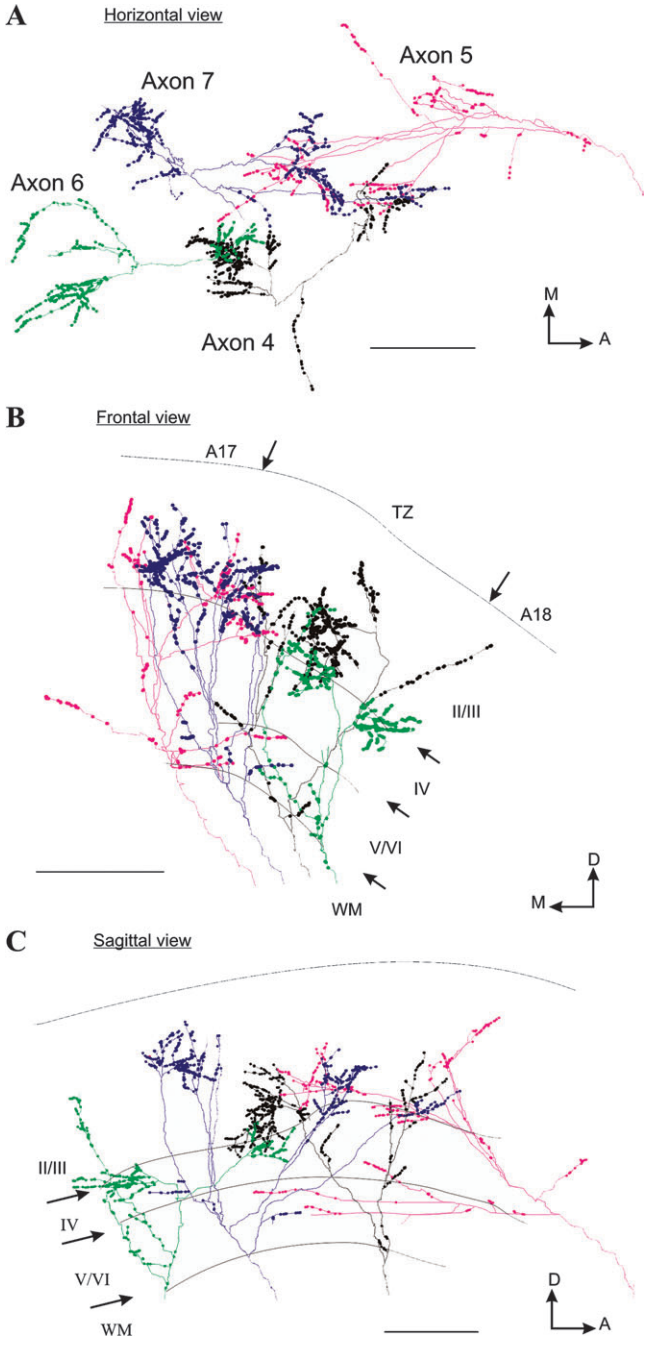

Figure 3. Three-dimensional reconstructions of four callosal axons originating from two neighboring injection sites. (*A–C*) Horizontal, frontal and sagittal views of axons 4 and 5 from the first injection site and axons 6 and 7 from the second injection site in cat Ca09. Same legend as in Figure 2. Scale bars, 500 µm.

(Diao et al. 1990; Payne 1990), the axons projecting outside the TZ are expected to display broader terminal arbors than those projecting within the TZ (Olavarria 1996). Indeed, we observed that the axon with the broadest arbor was the one located in A17 (axon 2, Ca06) whereas the most compact axon (axon 8, Ca15), with closely neighboring clusters, was located within the TZ (Fig. 2, Table 2).

The precise organization of callosal connections was finally demonstrated by case Ca09 where two different tracers were injected at nearby locations of the left hemisphere. In the right hemisphere, the locations of the corresponding labeled axon terminals were shifted in the same direction and by the same distance as that separating their respective injection sites (Fig. 7*B*,*D*).

Axial Specificity of Callosal Connections

It has been shown in previous studies that long intra-areal horizontal connections labeled by focal tracer injections form elongated axon terminal fields which are often collinear with the representation of the preferred orientation at the center of the injection site (Bosking et al. 1997). As shown in the horizontal views of the axons in Figures 2 and 3, the distributions of the callosal terminal boutons were mostly elongated, due to the presence of two or three distinct clusters within each axon terminal arbor. We were interested in determining whether the specific organization described for horizontal intrahemispheric connections also applies to callosal (interhemispheric) connections. We determined the axis of elongation of the bouton distributions for each callosal terminal arbor (see Materials and methods). We defined the preferred axis of each distribution with respect to the TZ, and compared this axis to the preferred orientation at the corresponding injection sites.

The elongation of the callosal terminals distribution was also quantified (see note to Table 1). This measure of anisotropy was in all cases higher than 2, showing that all axonal arbors were indeed clearly elongated (see Table 1, last column). Figure 7*E* shows the axes of elongation (red lines) for 4 callosal axon arbors as viewed from the cortical surface. Axon 4 was, for example, elongated parallel to the TZ (dashed line), whereas axon 3 was elongated orthogonal to it. Considering the topographic map of visual space represented in this cortical region, the axis of elongation of axon 4 corresponded to the retinotopic representation of a vertical line (i.e., an iso-azimuth line), whereas that of axon 3 corresponded to the representation of a horizontal line (see Materials and methods and Supplementary Fig. 1). The double arrows in Figure 7*E* (gray) show, for comparison, the retinotopic image of the preferred orientation represented at the injection site in the opposite hemisphere (see Table 2).

Figure 7*F* illustrates the relationship between these two axes (red lines and gray arrows in Fig. 7*E*) for all callosal axons with, in ordinates, the preferred axis of the axon (defined as the angle between the elongation axis of the axons and the TZ) and, in abscissa, the preferred orientation at the corresponding injection sites. For six out of eight axon arbors (axons 1, 2, 4, 5, 6, 8), we found that the preferred axis of the callosal terminals was within ±30° of the axis corresponding to the preferred orientation at the injection sites (Fig. 7*F*, solid line). Interestingly, the preferred axis of axon 3 was almost perfectly perpendicular (90.4°) to the axis derived from the orientation preference at the injection site (Fig. 7*E*,*F*). Nevertheless, we found a good overall correlation between the two angles (dashed line in Fig. 7*F*, Pearson's correlation $r = 0.79$ for all axons; $r = 0.92$ without axon 3) suggesting that, in addition to iso-orientation preference (Fig. 5), colinearity is a likely principle of target selection for callosal axons.

Discussion

This study demonstrates that callosal connections between the cat visual areas 17 and 18 of both hemispheres display a highly specific functional organization. All eight axons that were investigated displayed two or three clusters of terminal synaptic boutons when

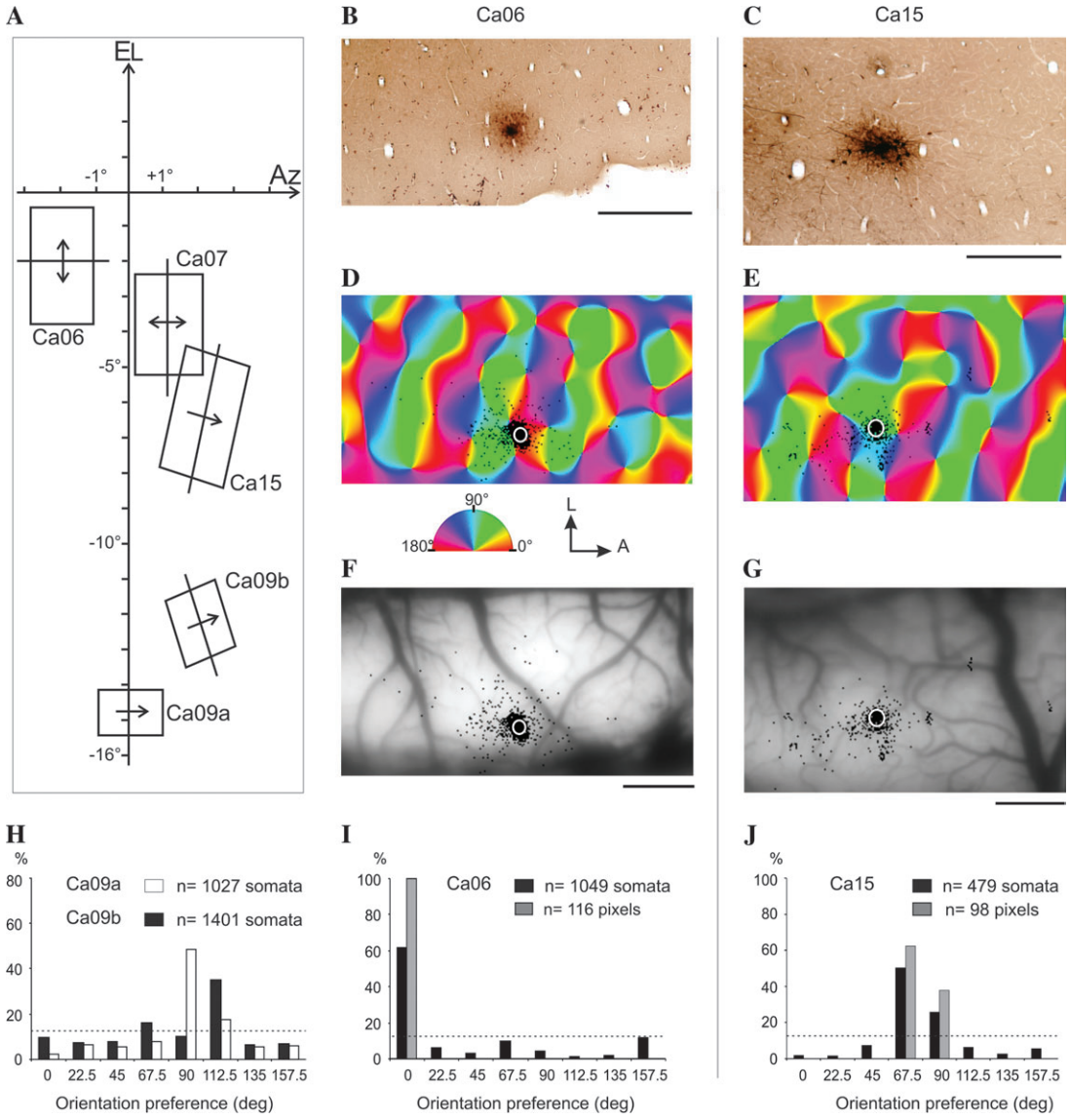

Figure 4. Analysis of the orientation preference at the injection sites (left hemispheres). (*A*) Location of the receptive fields, preferred orientation and preferred direction of the units recorded at the injection sites. These parameters were determined by multiunit recordings performed with the same glass pipettes that were used for iontophoretic injections. Only receptive fields of the units recorded with the stimulation of the contralateral eye (right eye) are presented. In cat Ca09, two injections were performed at different locations with two different tracers: injection site Ca09a with BDA and injection site Ca09b with FR. El, elevation; Az, azimuth. (*B*–*G*) Injection sites in cat Ca06 (left column) and cat Ca15 (right column). (*B*, *C*) Light microscopic images of the injection site (BDA). (*D*, *E*) Distribution of the labeled neuronal somata (in black) superimposed on orientation preference map (the preferred angle of a region is color-coded as indicated in the half circle). The injection core is indicated by a white circle. (*F*, *G*) Blood vessel pattern of the imaged region in (*D*) and (*E*) respectively. (*H*–*J*) Distribution of the labeled neuronal somata and of the pixels within the injection core in the different orientation domains (22.5° binning). Bars in (*H*) and black bars in (*I*) and (*J*) indicate the percentage of labeled neuronal somata. The distributions of the labeled neuronal somata in the different orientation domains were, in all cases, significantly centered on one orientation (*V*-test [modified Rayleigh test], $P < 0.01$). This orientation was defined as the orientation preference of the injection site: 90° for Ca09a (*H*), 112.5° for Ca09b (*H*), 0° for Ca06 (*I*), and 67.5° for Ca15 (*J*). Gray bars in (*I*) and (*J*) indicate the percentage of image pixels within the region of the injection core. The dotted line corresponds to the percentage of pixels that would be expected in each bin for an even distribution (12.5%). A, anterior; L, lateral. Scale bar, 500 μm (*B*, *C*); 1 mm (*F*, *G*).

viewed from the cortical surface. They all connected regions representing similar orientations and visuotopic locations within both hemispheres. Moreover, the axis of elongation of their termination fields correlated well with the preferred orientation of the site of origin in the opposite hemisphere.

Methodological Considerations

Completeness and Accuracy of Callosal Axon Reconstructions

All reconstructed axonal branches terminated with axonal swellings or boutons and were therefore likely filled until their distal ends. Under these experimental conditions, the anterograde transport of dextran tracers was more effective than their retrograde transport from one hemisphere to the other. Numerous callosal axonal branches were strongly labeled, whereas only a few labeled somata were observed in the hemisphere contralateral to the injection site. The relatively strong labeling of axons allowed us to quantify the total number of synaptic boutons, which ranged from 307 to 766. These numbers are higher than those previously reported for 3D-reconstructed callosal axons (labeled with biocytin) in the cat visual cortex (Houzel et al. 1994).

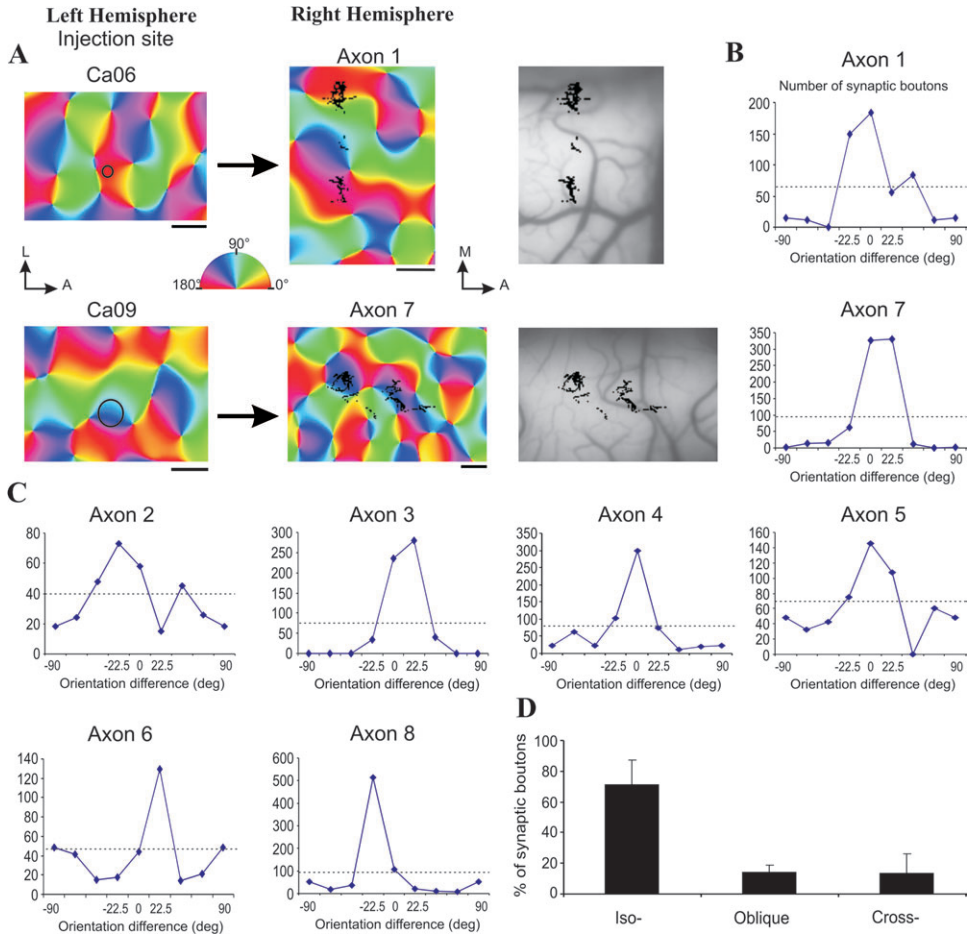

Figure 5. Modular specificity of callosal connections related to orientation preference. (*A*) Orientation preference maps with the location of the injection core (black circle) in the left hemisphere and the distribution of the synaptic boutons (in black) of a corresponding callosal axon in the right hemisphere (axon 1 in cat Ca06, axon 7 in cat Ca09). (*B*, *C*) Number of synaptic boutons of callosal axons in orientation domains. Orientation preferences were expressed relative to that of the injection sites using 22.5° resolution (0° corresponds to an orientation preference that is similar to that of the injection site; 90° corresponds to an orientation preference orthogonal to that of the injection site). The eight distributions have their peak at 0 ± 22.5°. The horizontal dotted line indicates for each axon the number of boutons that would be expected for an even distribution. (*D*) Percentages of synaptic boutons of callosal axons in iso- (±30°), oblique- (±30–60°), and cross- (±60–90°) orientation domains with respect to the orientation preference of the injection sites. The eight callosal axons connected preferentially iso-orientation domains with, in average, 72% (standard deviation = 17) of their synaptic boutons. Error bars indicate standard deviation. Scale bars 500 μm. A, anterior; M, medial; L, lateral.

Table 2

Distribution of labeled callosal axon terminals and callosal somata in iso- (±30°), oblique- (±30–60°) and cross- (±60–90°) orientation domains with respect to the orientation preference at the injection sites in the opposite hemisphere

Cat	Injection site (LH)		Callosal synaptic boutons (RH)					Callosal neuron somata (RH)			
	Orientation preference	Visual area	Axon number	Iso- (%)	Oblique (%)	Cross- (%)	Visual area	Number of somata	Iso- (%)	Oblique (%)	Cross- (%)
Ca06	0°	TZ	1	83	11	6	A17	8	63	13	24
			2	50	32	18	A17				
Ca07	90°	TZ	3	91	9	0	TZ	4	75	25	0
Ca09	90°	TZ	4	68	18	15	TZ	10	50	20	30
			5	51	18	31	TZ/A17				
	112.5°	TZ/A17	6	61	12	28	TZ	11	55	27	18
			7	92	7	2	TZ/A17				
Ca15	67.5°	A18	8	77	12	10	TZ	3	33	33	33
			Mean	72	15	14		Mean	55	24	21
			SD	17	8	11		SD	16	8	13

Note: The respective locations of injection sites and callosal axon terminals within A17, A18 and the transition zone between both areas (TZ) are indicated. LH, left hemisphere, RH, right hemisphere; SD: standard deviation.

In this previous study, nine out of seventeen callosal axons had less than 307 boutons and only four had more than 500 boutons.

Axon Diversity

It should be mentioned that the axons reconstructed in this study could represent a biased population because we might

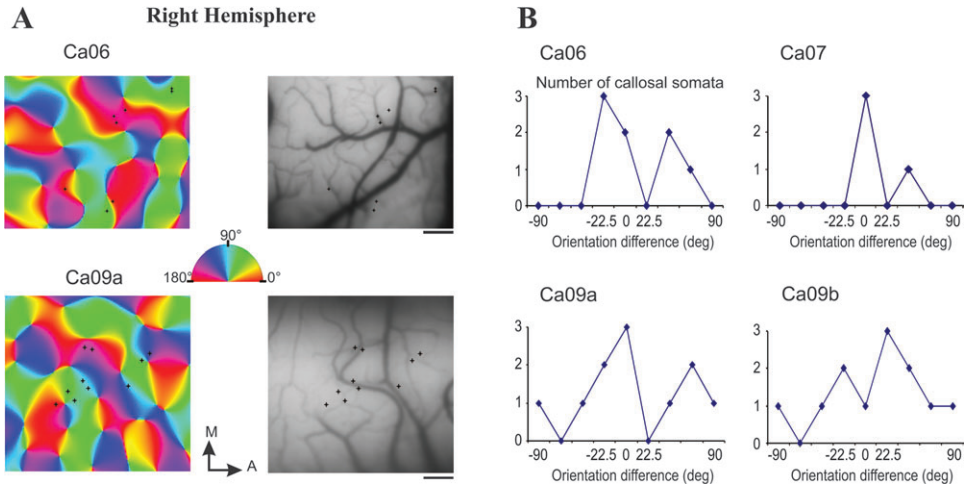

Figure 6. Distribution of retrogradely labeled somata of callosal neurons in orientation domains. (*A*) Neuronal somata are indicated by black stars superimposed on orientation preference maps of the right hemisphere of cats Ca06 and Ca09. Right panels: blood vessel patterns of the imaged regions. (*B*) Number of retrogradely labeled somata in orientation domains of the right hemisphere of cats Ca06, Ca07, and Ca09. Orientation preferences were expressed relative to that of the injection sites, as in Figure 5. Scale bars, 500 μm. A, anterior; M, medial; L, lateral.

have missed some thin callosal axons due to their faint labeling. A noteworthy feature of callosal axons is that they terminated mainly in the lower part of layer III and the upper part of layer IV. Only a few collaterals were encountered in deep layers (V and VI), and they almost completely avoided layer I. This laminar distribution confirms previous anatomical observations and electrophysiological recordings (Fisken et al. 1975; Shatz 1977; Innocenti 1980; Leporé and Guillemot 1982; Houzel et al. 1994; Milleret et al. 1994; Payne 1994). Finally, all reconstructed axons displayed at least one cluster of synaptic boutons (Houzel et al. 1994; Aggoun-Zouaoui et al. 1996).

Modular Specificity of Callosal Connections Related to Orientation Preference

The present study focused on the orientation specificity of single visual callosal axons. They were found to link regions of similar orientation preference (±30°) with an average of 72% of their synaptic boutons (Table 2), this proportion ranging from 50% to 92%. The heterogeneity in orientation preference seemed to be associated with morphological features of the axons. The two axons with the lowest percentages of iso-orientation connections had also the smallest numbers of synaptic boutons. As the quality of their labeling did not differ from that of the other axons, one possibility is that some branches established in the white matter were not reconstructed. Alternatively, the population of callosal axons may be heterogeneous in terms of orientation selectivity and subpopulations of these axons may serve different functions. For example, subpopulations could target different neuronal types, excitatory or inhibitory neurons because it has been shown that although callosal input is mainly excitatory, it can elicit both facilitatory and inhibitory responses in the targeted visual cortex (Payne et al. 1991; Makarov et al. 2008). Finally, it is also possible that the orientation specificity of callosal connections varies with the laminar location of the callosal neurons' somata (in layer II/III or in layer IV). Such variation has been observed in long-range intrahemispheric connections: layer II/III lateral connections preferentially link similar orientation domains whereas layer IV lateral connections link all orientation domains in a rather balanced manner (Yousef et al. 1999). This hypothesis could not be tested in the study reported here because extracellular neuronal tracer injections performed in the supragranular layers also labeled neurons in layer IV.

These results shed new light onto the organization of callosal connections with respect to orientation domains in mammalian visual cortex. Such selectivity has been investigated in only two previous studies, with another approach: retrograde labeling of callosal neurons after bulk injections of neuronal tracers. In tree shrew visual cortex (Bosking et al. 2000), callosal connections displayed only a very small bias toward linking sites of similar orientation preference. Contrary to this, in the visual cortex of strabismic cats, a significant bias of callosal connections was found for iso-orientations (Schmidt et al. 1997). The method we used here, that is, anterograde labeling and subsequent reconstructions of single callosal axons of normally reared cats, revealed marked iso-orientation specificity. The methodological difference between our and the above studies may in part explain the different result in terms of orientation selectivity. On the other hand, it is also likely that interhemispheric connectivity differs between tree shrew and cat, as it has already been shown for intrahemispheric connectivity (Fitzpatrick 1996). Our approach also revealed that the clustered organization of the callosal terminal arbors constitutes the main anatomical substrate for such functional specificity. The discovery of a discontinuous "columnar" pattern (or "clusters") of callosal terminals in rats and monkeys (Heimer et al. 1967; Künzle 1976; Jones et al. 1979) and later on in the cat visual cortex and other cortical areas (Berman and Payne 1983; Boyd and Matsubara 1994; Houzel et al. 1994; Innocenti 1986a; Voigt et al. 1988) raised the question of the functional specificity of such callosal terminal clusters. But none of these studies could establish a direct correlation between these clusters and the orientation maps of visual cortex. A significant bias was found in the distribution of callosal neurons' somata toward ocular dominance domains that were eye specific (Olavarria 2001); but see (Schmidt et al. 1997). It should be noted that the orientation selectivity of callosal connections we describe here does not contradict the

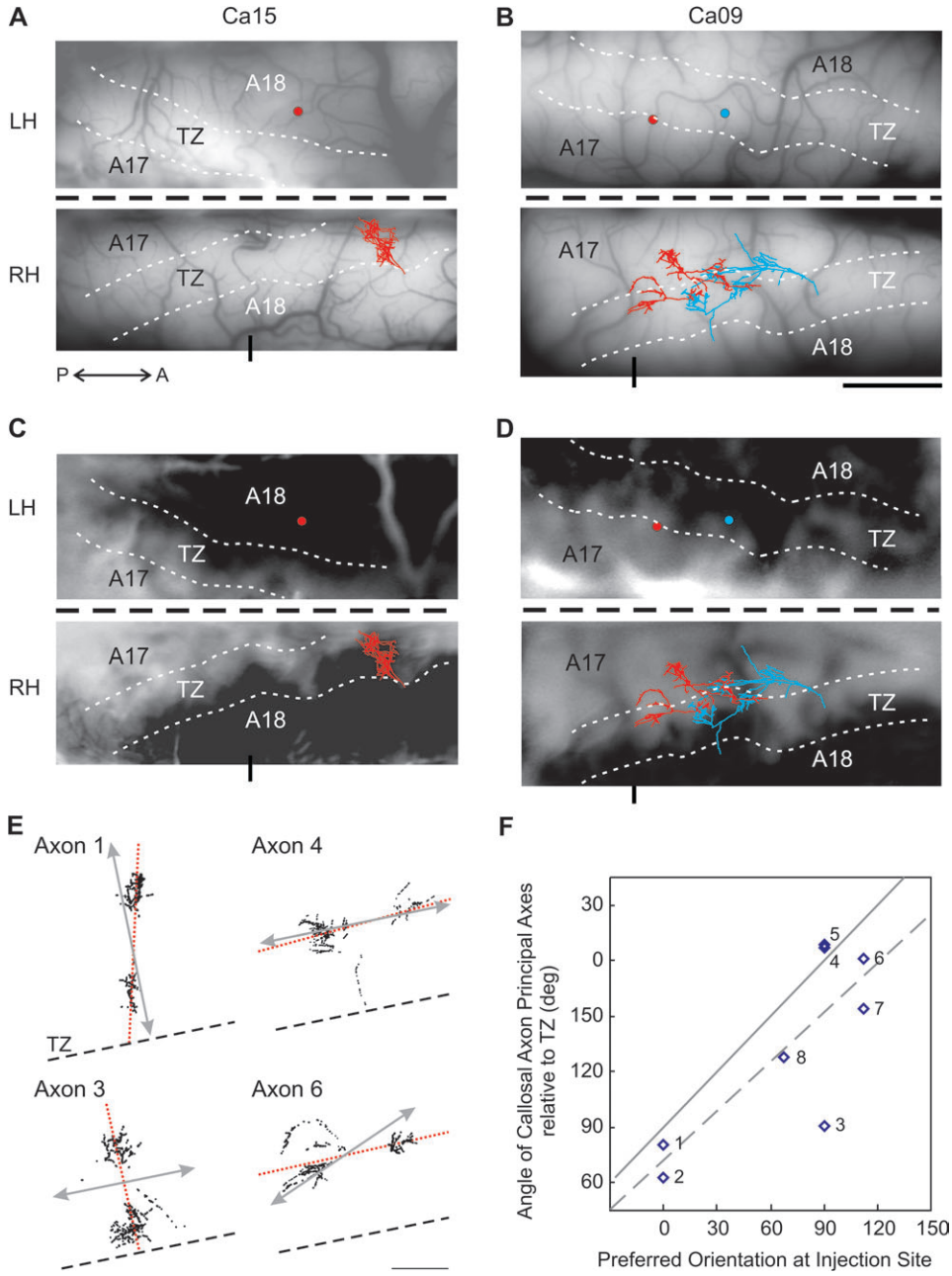

Figure 7. Visuotopic organization and axial specificity of callosal connections. (*A*, *B*) Overlap of the injection sites in the left hemisphere (LH) and the callosal axon terminals in the right hemisphere (RH) with images of the blood vessel pattern at the cortical surface. The reconstructed axon in Ca15 (*A*) is axon 8 (see detailed reconstruction in Fig. 2). In case of Ca09, two different tracers were injected at nearby locations (blue circle for injection site Ca09a and red one for Ca09b). In the opposite hemisphere, labeled axons coming from each injection site (red axons 4 and 5 for Ca09a and blue axons 6 and 7 for Ca09b) were shifted in the same direction and with the same distance as that separating their respective injection sites (see detailed reconstructions of these axons in Fig. 3). (*C*, *D*) Differential maps used to localize the transition zone between A17 and A18, in cats Ca15 (*A*) and Ca09 (*B*). The maps were obtained by dividing the sum of all SCMs imaged during the presentation of drifting gratings optimized for the activation of A18 (0.15 cpd, 4.5 Hz) by the sum of all SCMs imaged during the presentation of "A17-specific stimuli" (0.6 cpd, 1.5 Hz). Area 18 corresponds to the dark region. The anterior part of the cortex is on the right. The thick horizontal black dashed line shows the midline between both hemispheres; thin white dashed lines indicate the transition zone between A17 and A18 (TZ). Short vertical line at the bottom of each panel (in RH) shows stereotaxic coordinate AP0. The blood vessel patterns of the imaged regions are shown in (*A*) and (*B*), respectively. LH, left hemisphere; RH, right hemisphere; A, anterior; P, posterior. Scale bar, 2 mm. (*E*) Schemes illustrating the spatial distribution of callosal axon terminals (black dots) with respect to the axis of the 17/18 transition zone (black dashed lines). The schemes were rotated to align the TZs with each other. The red dashed lines indicate the principal axis of each axon's terminal field (first principal component of the set of *x* and *y* coordinates of the boutons). The double arrows (gray) represent the mapping of a retinotopic axis in A17 that corresponded to the preferred orientation at the injection site (e.g., 0° for axon 1; see Table 2). The examples show axons for which the principal axis of synaptic boutons distribution (red dashed lines) was approximately parallel (axons 1, 4, 6) or perpendicular (axon 3) to the axis derived from orientation preference (double arrows) at injection sites. Scale bars, 500 μm. (*F*) The angle between the preferred axis of the callosal axon terminals and the TZ was compared with the orientation preference at the corresponding injection site. The solid line shows the expected result if the preferred axes of callosal axons were perfectly parallel to the axes of preferred orientation at the injection sites. This simple prediction is based on the retinotopic map in A17 with the assumptions that iso-elevation and iso-azimuth lines are orthogonal to each other (see Supplementary Fig. 1) and that the magnification factor is equal in all directions. The dashed line indicates the linear fit to the data ($R^2 = 0.62$). Axon 3 was an outlier showing an elongation perpendicular to the predicted axis. The number of each axon (Tables 1 and 2, Figs 2 and 3) is indicated next to the data points.

hypothesis that these connections link regions with similar ocular dominance: callosal connections within an ocular dominance domain (or a binocular region) can also terminate in specific orientation domains.

The iso-orientation selectivity of callosal connections revealed in this study is consistent with electrophysiological data on split-chiasm cats showing that thalamo-cortical and callosal inputs can converge on the same cortical neuron and convey information about overlapping receptive fields with the same orientation tuning (Berlucchi and Rizzolatti 1968; Leporé and Guillemot 1982; Blakemore et al. 1983; Milleret et al. 1994, 2005; see review Houzel and Milleret 1999). This is also in agreement with recent optical imaging data demonstrating that both geniculo-cortical and callosal orientation maps overlap in the transition zone between A17 and A18, that is, where most callosal terminals are located (Rochefort et al. 2007). Furthermore, the specific connectivity of callosal axons provides an anatomical basis for the interhemispheric synchronization in the visual cortex (Engel et al. 1991). The most precise interhemispheric synchronization was found to occur almost exclusively between neurons with overlapping receptive fields (at least a partial overlap) and, in most cases, between neurons with similar optimal orientation preference (Nowak et al. 1995). After sectioning the corpus callosum, coupling was totally abolished (Nowak et al. 1995). More recent findings in human adult subjects have also shown that the interhemispheric coherence in the occipital brain regions increased (in the gamma frequency band) when the subjects viewed bilateral iso-oriented gratings located close to the vertical meridian of the visual field, or extending across it (Carmeli et al. 2005; Knyazeva et al. 2006).

Axial Specificity of Callosal Connections

The principal axis of elongation of the callosal axon terminal fields correlated with the axis corresponding to the preferred orientation at the injection sites, as represented in the visuotopic map of the opposite hemisphere. In six of the eight callosal axons, the principal axis of elongation was within 30° of the preferred orientation and only one axon (axon 3) had its principal axis perpendicular to the preferred orientation (Fig. 7*E,F*). Both cases (parallel and orthogonal elongations) were described for feedback projections from A17 and A18 to cat dorsal LGN (Murphy et al. 1999). Axons with orthogonal elongations (like axon 3) could enhance responsiveness in anticipation of movement orientation or direction of a stimulus and thus may influence cortical orientation and direction selectivity.

The axial specificity and iso-orientation selectivity of callosal connections suggests similar organizational principles and functions of both callosal and intrahemispheric long-range horizontal connections in the cat visual cortex. Both types of long-range connections originate from and terminate on similar cell types (Innocenti 1986b), have a patchy termination pattern and preferentially link similar orientation domains (Gilbert and Wiesel 1989; Houzel et al. 1994; Kisvárday et al. 1997; Schmidt et al. 1997; Yousef et al. 1999). Callosal connections were found to connect preferentially ocular dominance columns serving the same eye (Olavarria 2001; but see Schmidt et al. 1997), whereas intrahemispheric horizontal connections show no significant preference for ocular dominance territories (Matsubara et al. 1987; Löwel and Singer 1992; Schmidt et al. 1997). Concerning the development of both types of long-range connections, inter- and intrahemispheric, it is hypothesized that they are stabilized between neurons displaying correlated activities (Innocenti and Frost 1979; Lund and Mitchell 1979; Luhmann et al. 1990; Callaway and Katz 1991; Milleret and Houzel 2001). The selectivity demonstrated in the present study as well as previous results obtained in strabismic cats lend support to the above hypothesis. The callosal connections presented here linked preferentially similar orientation domains and in strabismic animals, both callosal and intrahemispheric horizontal connections also connect preferentially cortical regions with the same orientation and the same ocular dominance selectivity (Löwel and Singer 1992; Schmidt et al. 1997).

Intrahemispheric long-range horizontal connections of layer II/III appear to be well suited for enhancing the response to collinear contour elements (Gilbert et al. 1996; Bosking et al. 1997). So, what may be the role of the collinear organization of callosal connections? One possible role of their axial alignment is that callosal axons foster synchronicity between cortical cells that respond to contours stretched across the two visual hemifields and, consequently, "highlight" them as binocularly coherent. In this regard, callosal axons may act in synergy with intracortical horizontal connections of V1 (tree shrew, Fitzpatrick 1996; Bosking et al. 1997; new world monkey, Sincich and Blasdel 2001) and also with feedback projections from higher visual cortical areas to V1 (owl monkey; Shmuel et al. 2005). Hence, callosal connections may establish a specific network that links the representation of similar features between the two hemispheres, thus facilitating the fusion of the two visual hemifields into a single visual percept.

Supplementary Material

Supplementary material can be found at: http://www.cercor.oxfordjournals.org/.

FUNDING

Deutsche Forschungsgemeinschaft (SFB 509/A6) to Z.F.K.; the European Community (FP6-2004-IST-FETPI015879) to Z.F.K.; the Hungarian Academy of Sciences (TKI-242) to Z.F.K.; CNRS and the MENSER (ACI Neurosciences intégratives et computationnelles) to C.M.; and MENSER, the Fédération des Aveugles et Handicapés Visuels de France, and the International Graduate School of Neuroscience (IGSN) of Ruhr-Universität supported N.R.

Notes

We would like to thank Krisztina Kovács, Alex S. Ferecskó, Éva Tóth, and Anne-Marie Lampe for their support and their assistance during the optical imaging recordings and for histological processing. *Conflict of Interest*: None declared.

Address correspondence to Nathalie Rochefort, Institute of Neuroscience of the Technical University Munich, Biedersteiner Str.29, D-80802 Munich, Germany. Email: nathalie.rochefort@lrz.tu-muenchen.de.

References

Adams JC. 1981. Heavy metal intensification of DAB-based HRP reaction product. J Histochem Cytochem. 29:775.

Aggoun-Zouaoui D, Kiper DC, Innocenti GM. 1996. Growth of callosal terminal arbors in primary visual areas of the cat. Eur J Neurosci. 8:1132–1148.

Alekseenko SV, Toporova SN, Makarov FN. 2005. Neuronal connection of the cortex and reconstruction of the visual space. Neurosci Behav Physiol. 35:435–442.

[AQ3] Batschelet E. 1981. Circular statistics in biology. London.

Berlucchi G, Gazzaniga MS, Rizzolatti G. 1967. Microelectrode analysis of transfer of visual information by the corpus callosum. Arch Ital Biol. 105:583–596.

Berlucchi G, Rizzolatti G. 1968. Binocularly driven neurons in visual cortex of split-chiasm cats. Science. 159:308–310.

Berman NE, Payne BR. 1983. Alterations in connections of the corpus callosum following convergent and divergent strabismus. Brain Res. 274:201–212.

Bishop PO, Henry GH, Smith CJ. 1971. Binocular interaction fields of single units in the cat striate cortex. J Physiol. 216:3068.

Bishop PO, Kozak W, Vakkur GJ. 1962. Some quantitative aspects of the cat's eye: axis and plane of reference, visual field co-ordinates and optics. J Physiol. 163:466–502.

Blakemore C, Diao YC, Pu M, Wang Y, Xiao Y. 1983. Possible functions of the interhemispheric connexions between visual cortical areas in the cat. J Physiol. 337:331–349.

Bonhoeffer T, Grinvald A. 1993. The layout of iso-orientation domains in area 18 of cat visual cortex: optical imaging reveals a pinwheel-like organization. J Neurosci. 13:4157–4180.

Bonhoeffer T, Grinvald A. 1996. Optical imaging based on intrinsic signals: the methodology. In: Toga AW, Mazziotta JC, editors. Brain mapping: the methods. San Diego: Academic Press. p. 55–97.

Bonhoeffer T, Kim DS, Malonek D, Shoham D, Grinvald A. 1995. Optical imaging of the layout of functional domains in area 17 and across the area 17/18 border in cat visual cortex. Eur J Neurosci. 7:1973–1988.

Bosking WH, Kretz R, Pucak ML, Fitzpatrick D. 2000. Functional specificity of callosal connections in tree shrew striate cortex. J Neurosci. 20:2346–2359.

Bosking WH, Zhang Y, Schofield B, Fitzpatrick D. 1997. Orientation selectivity and the arrangement of horizontal connections in tree shrew striate cortex. J Neurosci. 17:2112–2127.

Boyd J, Matsubara JA. 1994. Tangential organization of callosal connectivity in the cat's visual cortex. J Comp Neurol. 347:197–210.

Buzás P, Eysel UT, Adorjan P, Kisvarday ZF. 2001. Axonal topography of cortical basket cells in relation to orientation, direction, and ocular dominance maps. J Comp Neurol. 437:259–285.

Buzás P, Eysel UT, Kisvárday ZF. 1998. Functional topography of single cortical cells: an intracellular approach combined with optical imaging. Brain Res Protoc. 3:199–208.

Buzás P, Kovacs K, Ferecsko AS, Budd JM, Eysel UT, Kisvarday ZF. 2006. Model-based analysis of excitatory lateral connections in the visual cortex. J Comp Neurol. 499:861–881.

Callaway EM, Katz LC. 1991. Effects of binocular deprivation on the development of clustered horizontal connections in cat striate cortex. Proc Natl Acad Sci USA. 88:745–749.

Carmeli C, Knyazeva MG, Innocenti GM, De FO. 2005. Assessment of EEG synchronization based on state-space analysis. Neuroimage. 25:339–354.

Carmeli C, Lopez-Aguado L, Schmidt KE, De FO, Innocenti GM. 2007. A novel interhemispheric interaction: modulation of neuronal cooperativity in the visual areas. PLoS ONE. 2:e1287.

Chisum HJ, Mooser F, Fitzpatrick D. 2003. Emergent properties of layer 2/3 neurons reflect the collinear arrangement of horizontal connections in tree shrew visual cortex. J Neurosci. 23:2947–2960.

Choudhury BP, Whitteridge D, Wilson M. 1965. The function of the callosal connections of the visual cortex. Q J Exp Physiol Cogn Med Sci. 50:214–219.

Chow KL, Lindsley DF. 1968. Influences of residual eye movements in single-unit studies of the visual system. Brain Res. 8:385–388.

Diao YC, Jia W, Swindale NV, Cynader MS. 1990. Functional organization of the cortical 17/18 border region in the cat. Exp Brain Res. 79:271–282.

Engel AK, König P, Kreiter AK, Singer W. 1991. Interhemispheric synchronization of oscillatory neuronal responses in cat visual cortex. Science. 252:1177–1179.

Fisken RA, Garey LJ, Powell TPS. 1975. The intrinsic, association and commissural connections of area 17 of the visual cortex. Philos Trans R Soc Lond B. 272:487–536.

Fitzpatrick D. 1996. The functional organization of local circuits in visual cortex: insights from the study of tree shrew striate cortex. Cereb Cortex. 6:329–341.

Gilbert C, Wiesel TN. 1989. Columnar specificity of instrinsic horizontal and corticocortical connections in cat visual cortex. J Neurosci. 9:2432–2442.

Gilbert CD, Das A, Ito M, Kapadia M, Westheimer G. 1996. Spatial integration and cortical dynamics. Proc Natl Acad Sci USA. 93:615–622.

Hancock MB. 1984. Vizualization of peptide-immunoreactive processes on serotonin- immunoreactive cells using two-color immunoperoxidase staining. J Histochem Cytochem. 32:311–314.

Heimer L, Ebner FF, Nauta WJ. 1967. A note on the termination of commissural fibers in the neocortex. Brain Res. 5:171–177.

Houzel JC, Milleret C. 1999. Visual inter-hemispheric processing: constraints and potentialities set by axonal morphology. J Physiol Paris. 93:271–284.

Houzel JC, Milleret C, Innocenti GM. 1994. Morphology of callosal axons interconnecting areas 17 and 18 of the cat. Eur J Neurosci. 6:898–917.

Hubel DH, Wiesel TN. 1967. Cortical and callosal connections concerned with the vertical meridian of visual fields in the cat. J Neurophysiol. 30:1561–1573.

Innocenti GM. 1980. The primary visual pathway through the corpus callosum: morphological and functional aspects in the cat. Arch ital Biol. 118:124–188.

Innocenti GM. 1986a. General organization of callosal connections in the cerebral cortex. In: Peters A, Jones EG, editors. Cerebral cortex. New York: Plenum. p. 291–353.

Innocenti GM. 1986b. Postnatal development of corticocortical connections. Ital J Neurol Sci Suppl. 5:25–28.

Innocenti GM, Frost DO. 1979. Effects of visual experience on the maturation of the efferent system to the corpus callosum. Nature. 280:231–234.

Jones EG, Coulter JD, Wise SP. 1979. Commissural columns in the sensory-motor cortex of monkeys. J Comp Neurol. 188:113–135.

Kiper DC, Knyazeva MG, Tettoni L, Innocenti GM. 1999. Visual stimulus-dependent changes in interhemispheric EEG coherence in ferrets. J Neurophysiol. 82:3082–3094.

Kisvarday ZF. 1992. GABAergic networks of basket cells in the visual cortex. Prog Brain Res. 90:385–405.

Kisvárday ZF, Eysel UT. 1992. Cellular organization of reciprocal patchy networks in layer III of cat visual cortex (area 17). Neuroscience. 46:275–286.

Kisvárday ZF, Ferecsko AS, Kovacs K, Buzás P, Budd JM, Eysel UT. 2002. One axon-multiple functions: specificity of lateral inhibitory connections by large basket cells. J Neurocytol. 31:255–264.

Kisvárday ZF, Toth E, Rausch M, Eysel UT. 1997. Orientation-specific relationship between populations of excitatory and inhibitory lateral connections in the visual cortex of the cat. Cereb Cortex. 7:605–618.

Knyazeva MG, Fornari E, Meuli R, Innocenti G, Maeder P. 2006. Imaging of a synchronous neuronal assembly in the human visual brain. Neuroimage. 29:593–604.

Künzle H. 1976. Alternating afferent zones of high and low axon terminal density within the macaque motor cortex. Brain Res. 106:365–370.

Leporé F, Guillemot JP. 1982. Visual receptive field properties of cells innervated through the corpus callosum in the cat. Exp Brain Res. 46:413–424.

Löwel S, Singer W. 1992. Selection of intrinsic horizontal connections in the visual cortex by correlated neuronal activity. Science. 255: 209–212.

Luhmann HJ, Singer W, Martinez-Millan L. 1990. Horizontal interactions in cat striate cortex: I. Anatomical substrate and postnatal development. Eur J Neurosci. 2:344–357.

Lund RD, Mitchell DE. 1979. The effects of dark-rearing on visual callosal connections of cats. Brain Res. 167:172–175.

Makarov VA, Schmidt KE, Castellanos NP, Lopez-Aguado L, Innocenti GM. 2008. Stimulus-dependent interaction between the visual areas 17 and 18 of the 2 hemispheres of the ferret (Mustela putorius). Cereb Cortex. 18:1951–1960.

Malach R, Tootell RB, Malonek D. 1994. Relationship between orientation domains, cytochrome oxidase stripes, and intrinsic horizontal connections in squirrel monkey area V2. Cereb Cortex. 4:151–165.

Matsubara JA, Cynader MS, Swindale NV. 1987. Anatomical properties and physiological correlates of the intrinsic connections in cat area 18. J Neurosci. 7:1428–1446.

Milleret C, Buser P. 1993. Reorganization processes in the visual cortex also depend on visual experience in the adult cat. Prog Brain Res. 95:257–269.

Milleret C, Buser P, Watroba L. 2005. Unilateral paralytic strabismus in the adult cat induces plastic changes in interocular disparity along the visual midline: contribution of the corpus callosum. Vis Neurosci. 22:325–343.

Milleret C, Houzel JC. 2001. Visual interhemispheric transfer to areas 17 and 18 in cats with convergent strabismus. Eur J Neurosci. 13:137–152.

Milleret C, Houzel JC, Buser P. 1994. Pattern of development of the callosal transfer of visual information to cortical areas 17 and 18 in the cat. Eur J Neurosci. 6:193–202.

Murphy PC, Duckett SG, Sillito AM. 1999. Feedback connections to the lateral geniculate nucleus and cortical response properties. Science. 286:1552–1554.

Nowak LG, Munk MHJ, Nelson JI, James AC, Bullier J. 1995. Structural basis of cortical synchronization. I. Three types of interhemispheric coupling. J Neurophysiol. 74:2379–2400.

Ohki K, Matsuda Y, Ajima A, Kim DS, Tanaka S. 2000. Arrangement of orientation pinwheel centers around area 17/18 transition zone in cat visual cortex. Cereb Cortex. 10:593–601.

Olavarria JF. 1996. Non-mirror symmetric patterns of callosal linkages in areas 17 and 18 in cat visual cortex. J Comp Neurol. 366:643–655.

Olavarria JF. 2001. Callosal connections correlate preferentially with ipsilateral cortical domains in cat areas 17 and 18, and with contralateral domains in the 17/18 transition zone. J Comp Neurol. 433:441–457.

Olavarria JF, Abel PL. 1996. The distribution of callosal connections correlates with the pattern of cytochrome oxidase stripes in visual area V2 of macaque monkeys. Cereb Cortex. 6:631–639.

Payne BR. 1990. Representation of the ipsilateral visual field in the transition zone between areas 17 and 18 of the cat's cerebral cortex. Vis Neurosci. 4:445–474.

Payne BR. 1994. Neuronal interactions in cat visual cortex mediated by the corpus callosum. Behav Brain Res. 64:55–64.

Ratzlaff EH, Grinvald A. 1991. A tandem-lens epifluorescence macroscope: hundred-fold brightness advantage for wide-field imaging. J Neurosci Methods. 36:127–137.

Rochefort NL, Buzas P, Kisvarday ZF, Eysel UT, Milleret C. 2007. Layout of transcallosal activity in cat visual cortex revealed by optical imaging. Neuroimage. 36:804–821.

Rochefort NL, Buzás P, Quenech'du N, Koza A, Milleret C, Kisvárday ZF. 2005. Orientation selectivity of interhemispheric connections in the cat visual cortex. Washington (DC): Society for Neuroscience Program No. 854.7.

Schmidt KE, Kim DS, Singer W, Bonhoeffer T, Löwel S. 1997. Functional specificity of long-range intrinsic and interhemispheric connections in the visual cortex of strabismic cats. J Neurosci. 17:5480–5492.

Shatz CJ. 1977. Anatomy of interhemispheric connections in the visual system of Boston Siamese and ordinary cats. J Comp Neurol. 173: 497–518.

Shmuel A, Korman M, Sterkin A, Harel M, Ullman S, Malach R, Grinvald A. 2005. Retinotopic axis specificity and selective clustering of feedback projections from V2 to V1 in the owl monkey. J Neurosci. 25: 2117–2131.

Sincich LC, Blasdel GG. 2001. Oriented axon projections in primary visual cortex of the monkey. J Neurosci. 21:4416–4426.

Somogyi P, Freund TF. 1989. Immunocytochemistry and synaptic relationships of physiologically characterized HRP-filled neurons. In: Heimer L, Zaborszky L, editors. Neuroanatomical tract-tracing methods 2: recent progress. New York: Plenum Press. p. 239–264.

Tusa RJ, Palmer LA, Rosenquist AC. 1978. The retinotopic organization of area 17 (striate cortex) in the cat. J Comp Neurol. 177:213–236.

Tusa RJ, Rosenquist AC, Palmer LA. 1979. Retinotopic organization of areas 18 and 19 in the cat. J Comp Neurol. 185:657–678.

Voigt T, LeVay S, Stamnes MA. 1988. Morphological and immunocytochemical observations on the visual callosal projections in the cat. J Comp Neurol. 272:450–460.

Yousef T, Bonhoeffer T, Kim DS, Eysel UT, Tóth É, Kisvárday ZF. 1999. Orientation topography of layer 4 lateral networks revealed by optical imaging in cat visual cortex (area 18). Eur J Neurosci. 11:4291–4308.